CHALMERS
UNIVERSITY OF TECHNOLOGY

Experimental Characterization of Dynamic Electrical Loading for Structural Battery Applications

Master's Thesis in Sustainable Electric Power Engineering and Electromobility

SURANJAN SAMANTA SANJEEV DESHPANDE

DEPARTMENT OF INDUSTRIAL AND MATERIALS SCIENCE
CHALMERS UNIVERSITY OF TECHNOLOGY
Gothenburg, Sweden 2026
www.chalmers.se

Master's thesis 2026

Experimental Characterization of Dynamic Electrical Loading for Structural Battery Applications

SURANJAN SAMANTA
SANJEEV DESHPANDE

Department of Industrial and Materials Science
Division of Production Systems
Chalmers University of Technology
Gothenburg, Sweden 2026

Experimental Characterization of Dynamic Electrical
Loading for Structural Battery Applications
SURANJAN SAMANTA
SANJEEV DESHPANDE

Supervisor: Ellinor Jansson , Department of Industrial and Materials Science
Examiner: Björn Johansson , Department of Industrial and Materials Science

Master's Thesis 2026
Department of Industrial and Materials Science
Division of Production Systems
Chalmers University of Technology
SE-412 96 Gothenburg
Telephone +46-317721000

Typeset in LaTeX
Printed by Chalmers Reproservice
Gothenburg, Sweden 2026

Experimental Characterization of Dynamic Electrical Loading for Structural Battery Applications
SURANJAN SAMANTA
SANJEEV DESHPANDE
Department of Industrial and Materials Science
Chalmers University of Technology

Abstract

Structural batteries, a recently developed technology, aims to combine energy storage and load-bearing capabilities within a single material system. Since early-stage structural battery prototypes are expected to be developed for small-scale applications before implementation in full-sized vehicles, there is a need for representative electrical loading conditions, operating requirements, and testing methodologies suitable for prototype development and evaluation.

In this thesis, commercial 1:10 scale RC vehicle platforms were used as experimental platforms to investigate realistic electrical demands associated with small-scale mobility applications. Current and voltage measurements were collected during both sustained full-load operation and representative dynamic driving conditions in order to capture realistic mobility-related electrical behaviour. The measured data was analysed to characterize the sustained and transient current demand of both platforms, which were further used to develop representative electrical drive cycles. The resulting drive cycles establish representative operating requirements for future structural battery prototypes intended for these applications, while simultaneously providing a repeatable dynamic testing profile for prototype evaluation.

Keywords: Structural Batteries, Prototype Evaluation, Drive Cycle, Small-Scale Mobility, RC Vehicles, Electrical Loading, Transient Response, Dynamic Testing, Electronic Load, Test Bench

Acknowledgements

We would first like to express our sincere gratitude to our supervisor, Ellinor Jansson, for her continuous guidance, valuable feedback, and support throughout the course of this master's thesis. Her input was fundamental in shaping the direction and completion of this work.

We would also like to acknowledge and thank the Production Systems Laboratory (PSL) for providing us with a dedicated workspace for the thesis work and for occasionally providing prototyping equipment that supported the experimental development process. In addition, we would like to thank the Chalmers Autonomous Systems and Electronics (CASE) Lab for allowing us to use their equipment. Access to these resources enabled the completion of this thesis.

Finally, we are thankful to Chalmers University of Technology for providing an excellent academic environment in which to work and pursue our interests.

Suranjan Samanta, Gothenburg, June 2026
Sanjeev Deshpande, Gothenburg, June 2026

List of Acronyms

Below is the list of acronyms that have been used throughout this thesis listed in alphabetical order:

ADC	Analog-to-Digital Converter
ESC	Electronic Speed Controller
ETC	Electronic Testing Circuit
EV	Electric Vehicle
FUDS	Federal Urban Driving Schedule
LSB	Least Significant Bit
NiMH	Nickel Metal Hydride
PCB	Printed Circuit Board
RC	Radio Controlled
SFUDS	Simplified Federal Urban Driving Schedule

Contents

List of Figures

1
Introduction

1.1 Background:

Extended electrification across transport and consumer product segments is essential to reduce emissions and improve resource efficiency. In parallel, increasing demands for product customization place additional constraints on weight and geometry, requiring systems that are both lightweight and flexible in design. Conventional energy storage solutions often add significant mass and impose packaging limitations, which can hinder overall system efficiency.

Structural batteries address these challenges by combining energy storage and load-bearing capabilities within a single material system [6]. Unlike traditional batteries that serve only as power sources, structural batteries are multifunctional materials that simultaneously store electrical energy and carry mechanical loads. By integrating the enclosure functionality directly with the battery cells, structural batteries enable a significant reduction in overall system weight without compromising either structural integrity or electrochemical performance.

While the concept of structural batteries offers clear advantages, transitioning from material-level development to functional prototypes requires a thorough understanding of the electrical demands they will face in real applications. Electrical loading in practice is dynamic and application-specific, and early-stage prototypes need to be developed and evaluated against conditions that actually reflect this. However, despite the various concepts developed in recent years, the viability of structural batteries has been demonstrated mostly at the material or coupon level [7], and the electrical loading conditions required to evaluate them at the prototype level remain largely unaddressed. Methodologies needed to evaluate structural battery prototypes against realistic operational requirements have yet to be established, representing a gap that limits the ability to meaningfully connect prototype performance to real application demands.

The significance of this project therefore lies in establishing the application-driven electrical loading conditions needed to support early structural battery prototype development. Previous work has demonstrated the value of determining application-level electrical requirements to guide structural battery development [8]; however, no equivalent characterization exists for small-scale mobility platforms. Since structural battery prototypes are at an early stage of development and are expected to be developed and validated at a small scale before integration into full-sized vehicles, establishing representative loading conditions at this scale represents a necessary first step. Using 1:10 scale Radio Controlled (RC) vehicle platforms as representative small-scale mobility systems, this work experimentally characterizes realistic drivetrain electrical behaviour under both sustained and dynamic operating conditions. The resulting loading profiles and drive cycles provide representative electrical requirements for structural battery prototypes at this scale. Recent advances in structural battery composite technology [9] make establishing these requirements a timely and necessary contribution, and the laboratory replay methodology developed in this work provides the test infrastructure needed to apply them directly in future prototype evaluation.

1.2 Aim:

This thesis aims to experimentally investigate and characterize the dynamic electrical loading behaviour associated with small-scale mobility applications, in order to establish representative operating conditions and electrical loading requirements for future structural battery prototype development and evaluation.

Using 1:10 scale RC vehicle platforms as representative small-scale mobility systems, the work experimentally characterizes realistic electrical loading under both sustained and dynamic operating conditions across two drivetrain configurations representing different performance levels. The derived loading profiles are used to develop representative drive cycles capturing the transient and sustained electrical demands relevant for structural battery prototype development, and a laboratory replay methodology is established to enable future prototypes to be tested against these conditions without requiring direct vehicle integration.

The work focuses on:

- Characterizing sustained and transient electrical loading behaviour of small-scale RC vehicle drivetrains under representative operating conditions.
- Developing representative drive-cycle profiles from experimental small-scale vehicle operation that capture the dynamic loading behaviour relevant for structural battery prototype development.
- Establishing a laboratory drive-cycle replay methodology for future structural battery prototype evaluation under representative loading conditions.

1.3 Limitations:

- Lack of structural battery prototypes

Structural batteries are still under development and were not expected to be available for experimental testing within the time frame of this thesis. For this reason, the setup is validated using conventional batteries. While this allows evaluation of the methodology and repeatability of the setup, behaviour specific to structural batteries cannot be assessed.

- Electrical-only evaluation of battery behaviour

The scope of this thesis is limited to establishing representative electrical loading profiles derived from dynamic small-scale vehicle operation. Dynamic mechanical loading effects relevant to structural batteries — such as bending, vibration, or structural stress — and their influence on electrical behaviour are therefore not assessed, as this falls outside the electrical characterization scope of this work.

2

Experimental Setup

2.1 Platform Selection

RC vehicle platforms provide a practical and accessible means of studying realistic electrical loading behaviour under dynamic driving conditions at a small scale. Although significantly smaller and simpler than full-sized vehicles, 1:10 scale RC platforms retain the principal components found in electric mobility systems — including electric motors, electronic speed controllers, battery systems, and mechanical drivetrains — and have been used in previous research as scaled experimental platforms for studying electric vehicle dynamics and energy consumption [10]. This makes them a suitable choice for capturing realistic acceleration, transient loading, and varying power demand at the scale relevant to early structural battery prototype development.

Rather than selecting specific RC car models, the work focuses on standardized chassis platforms. The intention was not to investigate the behaviour of a particular vehicle model, but instead to establish representative electrical loading conditions associated with mobility setups. By selecting chassis platforms with different drivetrain layouts and performance characteristics, the study aims to compare operating behaviour using a more generalized approach.

2.1.1 MB-01 Chassis

The MB-01 chassis shown in Figure 2.1 was selected to represent a low- to medium-performance mobility platform intended for city-driving and general transportation applications. The platform utilizes a compact front-wheel-drive configuration with a wheelbase of 210 mm and a relatively moderate drivetrain setup. The chassis employs a double-wishbone suspension system together with a front-wheel-drive drivetrain arrangement, enabling realistic transient loading behaviour while maintaining a relatively low loading demand. [1]

Since conventional on-road vehicle representative RC platforms are relatively limited, the MB-01 chassis was considered a suitable approximation among the available options.

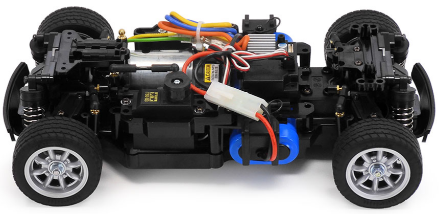

Figure 2.1: MB-01 Chassis [1]

2.1.2 TT-02 Chassis

The TT-02 chassis shown in Figure 2.2 was selected to represent a higher-performance mobility platform characterized by elevated transient power demand and increased torque requirements. The platform utilizes a shaft-driven four-wheel-drive configuration with a wheelbase of 257 mm and a longitudinal drivetrain layout designed to improve stability during high-performance operation. Compared to the MB-01 chassis, the TT-02 chassis is designed for more aggressive acceleration and higher dynamic loading conditions, making it suitable for investigating a higher loading demand. The chassis also employs a four-wheel double wishbone suspension system together with front and rear differential drivetrains, enabling stable high-load operation under dynamic driving conditions. [2]

Since high-performance mobility systems are considered a significant potential application area for structural batteries, the TT-02 platform was selected to investigate more demanding electrical loading behaviour associated with aggressive driving operation.

Figure 2.2: TT-02 Chassis [2]

2.2 Electronic Hardware

2.2.1 Powertrain

Both RC vehicle platforms used in this work were powered by a 7.2 V, 2500 mAh NiMH battery pack connected to a THW-1060-RTR Electronic Speed Controller (ESC) and a MABUCHI-540 brushed DC motor, with different drivetrain setups [1][2]. During operation, the ESC regulates the electrical power delivered from the battery to the motor according to the throttle input. Since the ESC operates through high-frequency switching of the motor supply, the resulting battery current is not constant and instead varies continuously during changing load conditions. This behaviour becomes particularly significant during experimental testing, where rapidly varying current demand and transient current spikes can be observed throughout the measured electrical loading profiles.

2.2.2 INA219 current/power sensor

2.2.2.1 Overview and Technical data

Since the objective of the work required simultaneous acquisition of current, voltage, and electrical power during dynamic vehicle operation, the INA219 digital current shunt and power monitor was selected as the primary sensing device for the experimental setup. Configured as shown in Figure 2.3, the INA219 communicates through an I^2C-compatible interface, allowing direct integration with the ESP32-based data acquisition system used in this work [3].

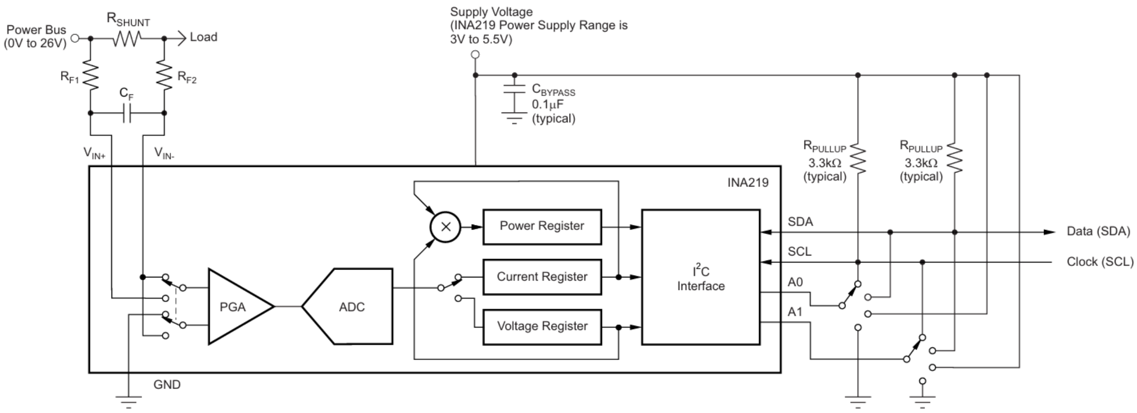

Figure 2.3: INA219 Sensor Schematic [3]

INA219 operates by measuring the differential voltage drop across an external shunt resistor in order to determine the current flowing through the system. In addition to current sensing, the INA219 is also capable of measuring the bus voltage, enabling real-time electrical power consumption to be calculated internally. The sensor supports bus voltage measurements up to 26 V while operating from a 3 V to 5.5 V supply voltage range, making it suitable for the 7.2 V NiMH battery systems used in the RC vehicle platforms.

INA219 also provides programmable measurement resolution and averaging functionality, allowing measurement filtering and stable acquisition under varying dynamic load conditions [3]. Compared to analog current sensing approaches, the digital I^2C interface simplified data acquisition and reduced susceptibility to analog signal noise during vehicle operation.

2.2.2.2 Programming the calibration Register

Calibration of the INA219 is required to scale the raw shunt voltage and bus voltage measurements into corresponding current and power values representative of the actual drivetrain loading. The calibration value is determined using the selected Current_LSB value together with the value of the external shunt resistor. Once the calibration register has been programmed, the Current Register (04h) and Power Register (03h) are automatically updated based on the measured shunt and bus voltages. Until calibration is performed, both the current and power registers remain at zero [3].

$$Cal = \text{trunc}\left[\frac{0.04096}{\text{Current\_LSB} \times R_{\text{SHUNT}}}\right] \tag{2.1}$$

Where: 0.04096 is an internal fixed value used to ensure scaling is maintained properly

$$Current\_LSB = [\frac{MaximumExpectedCurrent}{2^{15}}]. \tag{2.2}$$

$$CurrentRegister = [\frac{ShuntVoltageRegister \times CalibrationRegister}{4096}] \tag{2.3}$$

The Calibration Register value is calculated based on equation (2.1) [3]. This equation includes the term Current_LSB, which is the programmed value for the least significant bit (LSB) of the Current Register (04h). The highest resolution of the Current Register (04h) is achieved by selecting the smallest allowable Current_LSB value based on the maximum expected current, as shown in equation (2.2). The term R_SHUNT refers to the value of the external shunt resistance used to develop the differential voltage across the input pins. In this study, the shunt resistance value is 10 mΩ. The Power Register (03h) is internally configured to be 20 times the programmed Current_LSB.

Shunt voltage is calculated by multiplying the Shunt Voltage Register contents with the Shunt Voltage LSB of 10μV. The Bus Voltage register bits are not right-aligned. In order to compute the value of the Bus Voltage, Bus Voltage Register contents must be shifted right by three bits. This shift puts the BD0 bit in the LSB position so that the contents can be multiplied by the Bus Voltage LSB of 4mV to compute the bus voltage measured by the device. After programming the Calibration Register, the value expected in the Current Register (04h) can be calculated by multiplying the Shunt Voltage register contents by the Calibration Register and then dividing by 4096 as shown in (2.3). To obtain a value in amperes the Current register value is multiplied by the programmed Current_LSB.

The INA219 sensor was configured for a 16 V / 32 A operating range during experimental testing. According to the INA219 configuration register, the sensor only provides selectable bus-voltage full-scale ranges of 16 V and 32 V. Since the RC vehicle platforms operated using a 7.2 V battery system, the 16 V range represented the most suitable available measurement configuration while still providing sufficient operating headroom. Preliminary experimental measurements also indicated transient drivetrain current peaks approaching 32 A during aggressive dynamic vehicle operation,hence the current measurement range was therefore configured for 32 A operation using the maximum programmable shunt-voltage range of ±320 mV together with the selected shunt resistor calibration values. The corresponding calibration code is provided in Appendix A.1.

Accurate calibration of the sensor was particularly critical in this work due to the transient nature of the electrical loading behaviour being characterized. The initial current peak and corresponding voltage drop occurring during acceleration from rest represent the most demanding operating point of the drivetrain, and capturing these transient events accurately required careful configuration of the shunt ADC resolution and averaging settings. For the test platforms used in this work, the configuration "$INA219\_CONFIG\_SADCRES\_12BIT\_32S\_17MS$" was selected to balance measurement stability with sufficient resolution to capture these transient events. The corresponding calibration code and sample time configuration are provided in Appendix A.1 and Appendix A.2 respectively.

2.2.3 Electronic Test Circuit

Since the experimental platforms were dynamic and required onboard electrical monitoring during vehicle operation, a custom PCB-based data acquisition system was developed rather than relying on rapid prototyping alternatives. The Electronic Test Circuit (ETC) PCB, shown in Figure 2.4, was designed to interface directly between the battery pack and the ESC, enabling continuous measurement of drivetrain current, voltage, and power during dynamic vehicle operation.

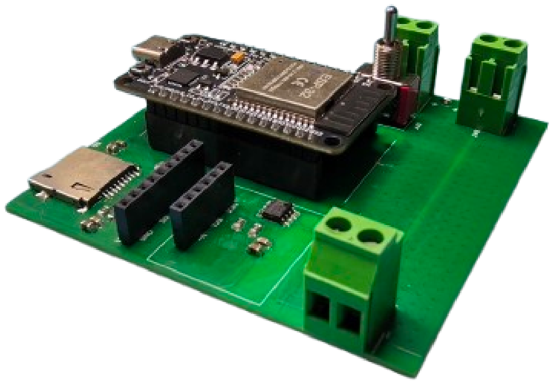

Figure 2.4: Electronic Test Circuit PCB

The PCB incorporates wide copper traces between the battery and ESC connections to support the high transient current demands generated during dynamic operation, in series with a shunt resistor network interfaced with the INA219 sensor. A resistor network was used in place of a single shunt resistor to distribute the power dissipation across multiple components, addressing the limited power rating of commercially available low-resistance shunt resistors at the current levels encountered during operation.

An ESP32 NodeMCU microcontroller [11] serves as the primary onboard data acquisition platform, continuously acquiring measurements from the INA219 sensor and storing the recorded data locally onto an SD card. Developing the ETC PCB enabled logging of electrical measurement data directly on the moving RC platform without requiring any external connection during testing. The ETC architecture was additionally designed with provision for future battery monitoring applications, including the possibility of integrating temperature sensors and external cutoff control, to be integrated into the test bench developed in Section 3.4

3
Methodology

This work followed an experimental methodology aimed at characterizing the dynamic electrical loading behaviour of small-scale RC vehicle platforms, in order to establish representative operating conditions and electrical loading requirements for future structural battery prototype development and evaluation. An onboard electrical measurement and data acquisition system was first integrated onto the selected RC vehicle platforms, after which sustained full-load and representative dynamic driving experiments were conducted to characterize both the transient and sustained drivetrain electrical behaviour. The measured loading profiles were then sequenced into representative drive cycles and replayable profiles, which were subsequently reproduced using a programmable electronic load under controlled laboratory conditions.

3.1 Electrical Characterization Approach

The electrical loading characterization in this work was performed using physical RC vehicle platforms, rather than relying on simulation or analytical estimation. Previous studies have demonstrated that battery performance evaluation conducted using experimentally obtained drive cycles can provide a more representative assessment, since dynamic operating conditions and transient drivetrain behaviour can significantly influence battery electrical response [12]. Additionally, capturing the genuine transient loading behaviour of the drivetrain was considered important for the development of representative drive cycle profiles, as discussed in Section 3.3.2. This was only possible by capturing the actual dynamic loading behaviour of the platforms during vehicle operation, as estimation of the loading behaviour would provide an approximation of only the sustained loading levels. Experimental characterization was therefore selected as the approach for developing representative electrical loading profiles in this thesis.

3.2 Platform Integration

Both RC vehicle platforms were assembled in their complete operational configurations prior to experimental testing. In addition to the drivetrain components, each platform was equipped with a CS-3 steering servo and a 3-channel mini receiver for vehicle operation. The ETC developed in this work was integrated onto both vehicle platforms above the main chassis structure, enabling onboard electrical measurement and data acquisition during testing. The final integrated experimental platforms are shown in the Figure 3.1.

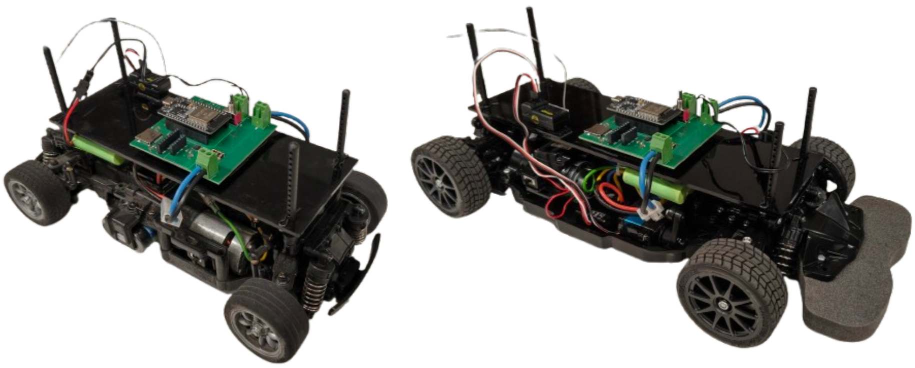

Figure 3.1: Integrated experimental platforms (Left - MB-01, Right - TT-02)

The onboard ESP32 data acquisition system continuously acquired current, voltage, and power measurements from the INA219 and stored the recorded data locally onto the onboard SD card during vehicle operation. The complete source code used for the experimental data acquisition system is provided in Appendix A.3.

3.3 Dynamic Testing

3.3.1 Full Load Testing

The first test performed on both RC vehicle platforms was a full-load battery discharge test, in which each platform was operated under continuous full-throttle input from a fully charged battery until complete discharge. The primary purpose of this test was to characterize the electrical loading behaviour of the RC vehicle drivetrains under continuous constant-load operation, in order to make informed decisions regarding the development of representative drive cycles for each platform.

During testing, the vehicles were operated from rest under constant full-throttle input until the battery could no longer sustain normal vehicle operation. The steering servo was also continuously actuated during testing to introduce additional dynamic loading conditions representative of normal RC platform operation.

Current, voltage, and power measurements were continuously recorded throughout the experiment using the onboard ETC developed in this thesis. Particular attention was given to observing the transient drivetrain behaviour during initial acceleration from rest, as well as the overall electrical loading behaviour of the drivetrain throughout the battery discharge process.

No dedicated cutoff system was implemented during the full-load test. Due to the switching behaviour of the ESC, large transient voltage drops occurred frequently during operation, making a simple voltage-threshold cutoff unreliable and potentially leading to premature termination during normal operation. The battery was considered fully discharged when the steering servo stopped responding and the drivetrain response became significantly weakened, signalling the end of normal vehicle operation.

The results of the full-load test were used to identify the dominant load characteristic of these platforms, inform the decision regarding the domain in which the drive cycles would be reproduced, and additionally establish the representative peak and sustained demands that future structural battery prototypes for these platforms would need to satisfy under continuous full-load operation.

3.3.2 Representative Drive Cycle Generation

Previous studies have shown that drive-cycle-derived loading can be used to relate vehicle-level operating requirements to battery material properties [13], which suggests drive-cycle-based electrical loading characterization would provide a suitable basis for the development of structural battery prototypes. Furthermore, variable drive cycle based testing has been established as the standard approach for evaluating EV battery performance under realistic operating conditions [14], suggesting that the same approach can be used to provide a repeatable testing methodology for structural battery prototype evaluation. So, following the full-load discharge testing, representative dynamic drive cycles were developed for both RC vehicle platforms. The purpose of this stage was to obtain realistic transient electrical loading profiles that could not only be used to study the electrical loading requirements of future structural battery prototypes, but could also later be reproduced on a laboratory test bench without requiring the structural battery prototypes to be directly integrated into the RC vehicle platforms themselves. [15]

Instead of operating the platforms in completely random driving behaviour, a representative commercial drive cycle was experimentally reproduced at a small scale. After reviewing existing studies on drive cycles used for EV battery testing applications, the SFUDS drive cycle shown in Figure 3.2 was selected as the reference profile. The studies identified SFUDS as a simplified drive cycle, derived from the standard FUDS profile, used for EV battery testing applications, consisting primarily of repeated acceleration, cruising, braking and idle regions [4] [16] [14]. The comparative simplicity of drive cycles such as SFUDS was considered suitable for early-stage battery development and evaluation [17], as the primary objective was to establish representative operating requirements and evaluate basic feasibility under controlled loading conditions rather than reproduce the full complexity of real-world vehicle operation. Additionally, Redey [18] has already demonstrated that the SFUDS profile can be used to measure the dynamic performance of research cells [18]. Hence, SFUDS seemed the most suitable profile for this thesis. However, it's worth noting that the objective was not to reproduce the exact vehicle motion representative of the SFUDS drive-cycle, but rather to reproduce representative drivetrain loading behaviour and throttle transitions corresponding to the drive-cycle profile. Consequently, vehicle operation was manually controlled to recreate the required acceleration, braking, and sustained throttle conditions associated with each section of the drive cycle instead of designing a set track layout.

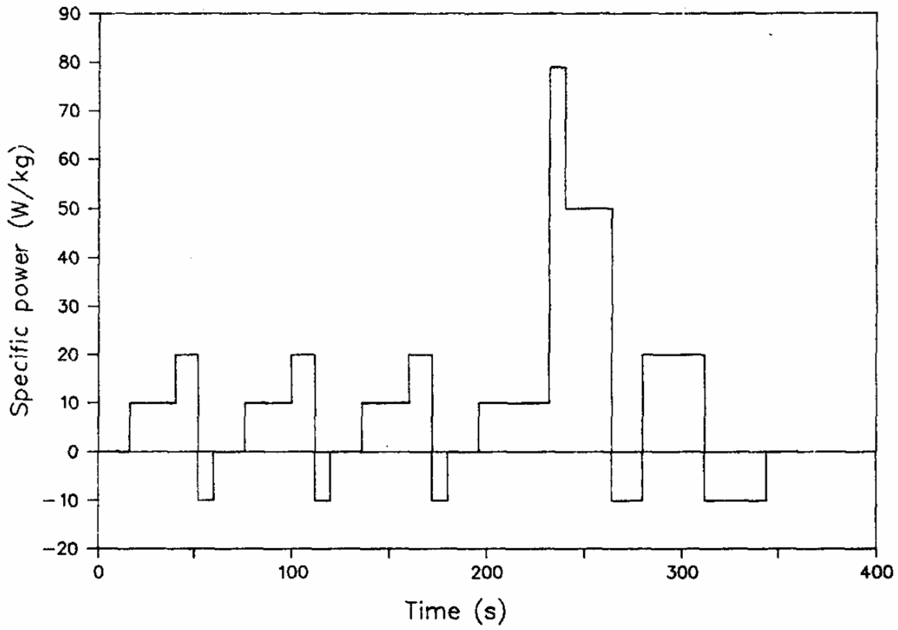

Figure 3.2: SFUDS drive cycle [4]

The original SFUDS drive cycle is defined in terms of specific power demand as can be seen in the Figure 3.2, as electric vehicle performance is determined primarily by the power characteristics, and therefore accurate evaluation of EV batteries is based on schedules in which power is the control variable [19]. Consequently, power-based drive cycles like SFUDS are used for the evaluation of EV batteries, and in order to meet the power demands throughout discharge, any fall in voltage must be matched by an increase in the current drawn from the battery [19]. However, as demonstrated by the full load testing results presented in Section 4.1, the RC drivetrain current remained approximately constant throughout discharge even as the battery voltage declined. The performance of these platforms is therefore characterized by current loading rather than power. Hence, the SFUDS-based drive cycle in this work was reproduced in terms of current rather than power.

The original SFUDS drive cycle is intended for full-scale road vehicles and hence the time scale needed to be scaled to obtain representative operating durations suitable for the 1:10 scaled RC platforms used in this work. Direct linear scaling of the original drive-cycle timing was not considered suitable since it excessively compressed the operating regions, creating the possibility of preventing the RC drivetrain from fully developing the representative transient loading behaviour. To determine the scaling factor, the dimensional analysis framework of Kumari et al.[10] was adopted as a basis. In their work, the Buckingham π theorem is applied to a bicycle model of vehicle dynamics, yielding a set of dimensionless groups that govern similarity between a scaled RC vehicle and a full-size vehicle. One of these groups, π_8, relates time to the vehicle's cornering stiffness C_F, wheelbase l, and mass m:

$$\pi_8 = \sqrt{\frac{C_F}{l \cdot m}} \cdot t = \text{constant} \tag{3.1}$$

which results in the following proportional relationship:

$$t \propto \sqrt{\frac{l \cdot m}{C_F}} \tag{3.2}$$

However, unlike Kumari et al., whose objective was to preserve vehicle dynamic similarity between the scaled and full-scale vehicles, the present work only aimed to obtain a practical approximation of the drive-cyle time scale, and complete dynamic similitude analysis was therefore considered outside the scope of the study. Consequently, an assumption was made that the ratio C_F/m remained approximately similar due to scaling proportionally between the scales, reducing the time scaling relationship to:

$$t \propto \sqrt{l} \tag{3.3}$$

For a scaling factor of λ = 1:10 for the RC vehicle platforms, the time axis of the SFUDS drive cycle was therefore compressed by a factor of:

$$\frac{t_{RC}}{t_{full}} = \sqrt{\lambda} = \sqrt{\frac{1}{10}} \approx 0.316 \tag{3.4}$$

Using this factor, the regions in the original SFUDS drive-cycle were proportionally reduced to obtain a scaled representative time scale for the RC vehicle platforms. The scaled drive cycles were then approximately reproduced through manual operation of the RC vehicles. Since regenerative braking was not possible with the RC vehicle powertrain, the reproduced loading profiles could not capture the negative electrical loading behaviour typically associated with regenerative braking in full-scale EVs. Consequently, the negative-power regions of the original SFUDS cycle from Figure 3.2 were instead replaced with zero-throttle coasting regions while maintaining the corresponding scaled timing intervals. As a result, the loading requirements developed in the present work are limited to driving conditions, while regenerative braking behaviour and associated bidirectional loading requirements remain outside the scope of the present study. It should be noted that the original SFUDS cycle also has specific proportional ratios between its loading levels, as can be seen in the Figure 3.2. Since the drive cycles in this work were reproduced through manual throttle operation, maintaining these exact proportional ratios between loading levels was not practically achievable. The objective of this study was rather to reproduce a dynamic loading pattern representative of the SFUDS structure.

During operation, the current measurements were continuously recorded using the ETC developed in this thesis. The raw current signals recorded from the RC car drivetrain contained high-frequency fluctuations due to ESC switching. The SFUDS drive cycle simplifies the continuously varying power demand of real urban driving into discrete constant-level steps [16]. Since the objective of the present work was to reproduce an SFUDS-representative drive cycle for the RC vehicle platforms, the measured current profiles were simplified into discrete constant-current segments, where each segment represents the average current within the corresponding operating region. However, the transient peaks and drops observed during drivetrain transitions have been preserved in the sequenced profiles, as transient drivetrain behaviour has been shown to significantly influence battery electrical response [12]. Preserving these peaks and drops was therefore considered relevant to ensure the drive cycle remained representative of the loading conditions that the battery prototypes would experience during testing, since future structural battery systems for these applications would need to tolerate not only sustained average loading conditions but also rapid short-duration current demand during dynamic operating transitions. The transient peaks and drops in the sequenced profiles have been preserved as ramped responses - fluctuating sharply before gradually settling toward the sustained average current level of the corresponding operating region.

3.4 Testbench and Drive-cycle Replay

Following the development of the representative drive-cycle current profiles, laboratory replay testing was conducted on a test bench developed using an EA Elektro-Automatik EL 9080-45 T programmable electronic load [20] and the ETC developed in this thesis configured as the electrical monitoring circuit 3.3.

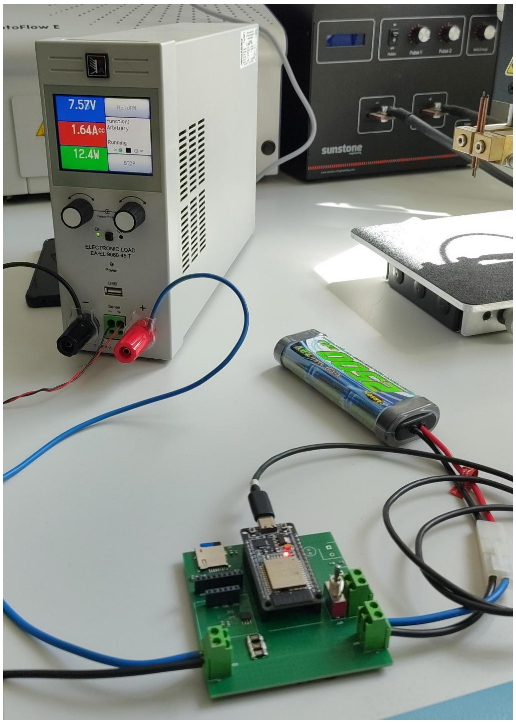

Figure 3.3: Test Bench

The purpose of this stage was to reproduce the experimentally obtained drivetrain loading behaviour under controlled laboratory conditions, allowing future structural battery prototypes to be tested without requiring direct integration into the RC vehicle platforms.

The EL 9080-45 T was selected for this purpose as its built-in arbitrary function generator supports up to 99 freely configurable sequence points [21], which was sufficient to accommodate the 41-step current profiles developed in this work 4.16 4.17. This approach provided a practical and repeatable means of replaying the simplified drive cycle profiles under controlled laboratory conditions.

The primary objective of the replay testing was to verify the replayability of the developed current profiles and to establish a ready test bench setup that can be used for the evaluation of the developed structural battery prototypes intended for same-scale applications in future work.

4
Results

4.1 Full Load Test

Figure 4.1 shows the characteristic discharge voltage behaviour of a NiMH battery under constant current discharge at varying C-rates [5]. The flat voltage plateau visible at lower discharge rates becomes progressively less defined as the C-rate increases. The voltage behaviour of both platforms during the full-load test is interpreted with reference to these characteristic curves in the following subsections.

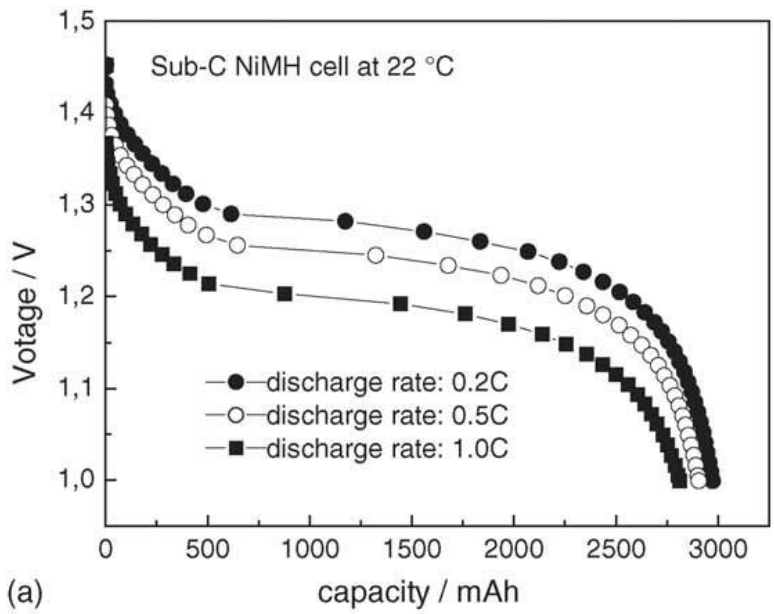

Figure 4.1: Characteristic NiMH Discharge Voltage Curves [5]

4.1.1 MB-01

The following subsections present the current, voltage, and power measurements recorded during the sustained full-load endurance test on the MB-01 platform.

4.1.1.1 Current Behaviour

Figures 4.2 and 4.3 show the measured current behaviour of the MB-01 platform during the sustained full-load endurance test. The raw current signal is presented alongside a smoothed trend obtained by applying a moving average filter, in order to separate the underlying average drivetrain current demand from the high-frequency switching fluctuations introduced by the ESC.

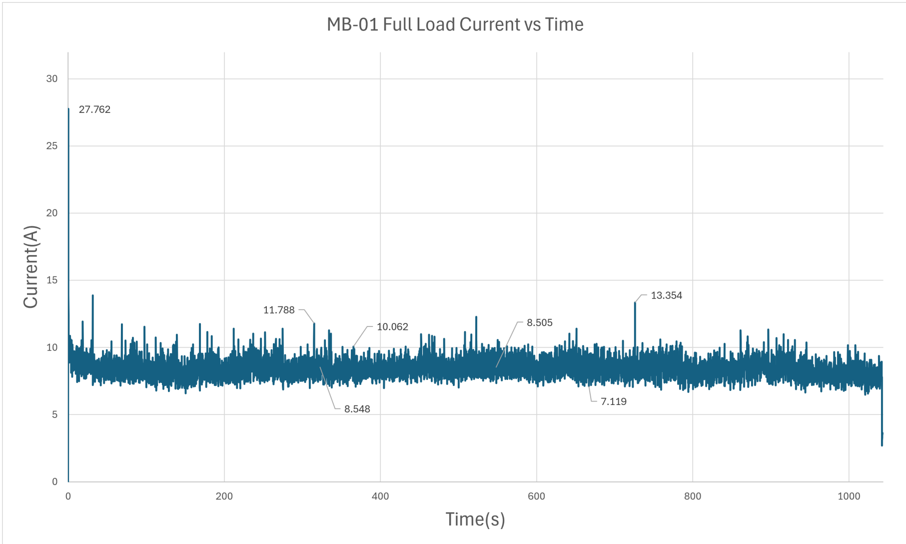

Figure 4.2: MB-01 Raw Full Load Current

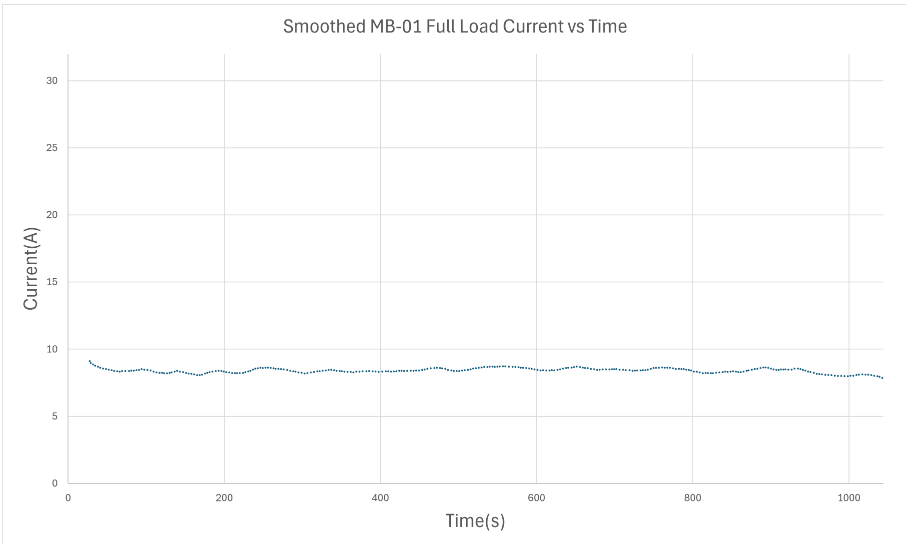

Figure 4.3: MB-01 Smoothed Full Load Current

The measured drivetrain current exhibited continuous high-frequency fluctuations throughout operation due to the switching behaviour of the ESC, resulting in repeated short-duration current peaks and drops during sustained operation. An initial instantaneous current peak of approximately 27.8 A was observed during acceleration from rest, visible as the sharp spike at the start of the raw current signal in Figure 4.2, after which the drivetrain settled into a relatively stable operating region as evident from the smoothed trend in Figure 4.3.

Although the raw current signal contained significant switching ripple between 7–12 A with a logging interval of approximately 110 ms, the smoothed current trend showed that the underlying average drivetrain current remained comparatively stable at approximately 8–9 A throughout most of the discharge process. This indicated that the overall drivetrain loading behaviour was characterized more by a relatively constant average current demand. However, the results also showed that future structural battery systems for these applications would require sufficient transient response capability to tolerate repeated high-frequency current fluctuations during operation.

4.1.1.2 Voltage Behaviour

Figures 4.4 and 4.5 show the voltage behaviour of the MB-01 platform battery throughout the sustained full-load endurance test. The raw voltage signal is presented alongside a smoothed trend obtained by applying a moving average filter to better illustrate the underlying battery discharge behaviour.

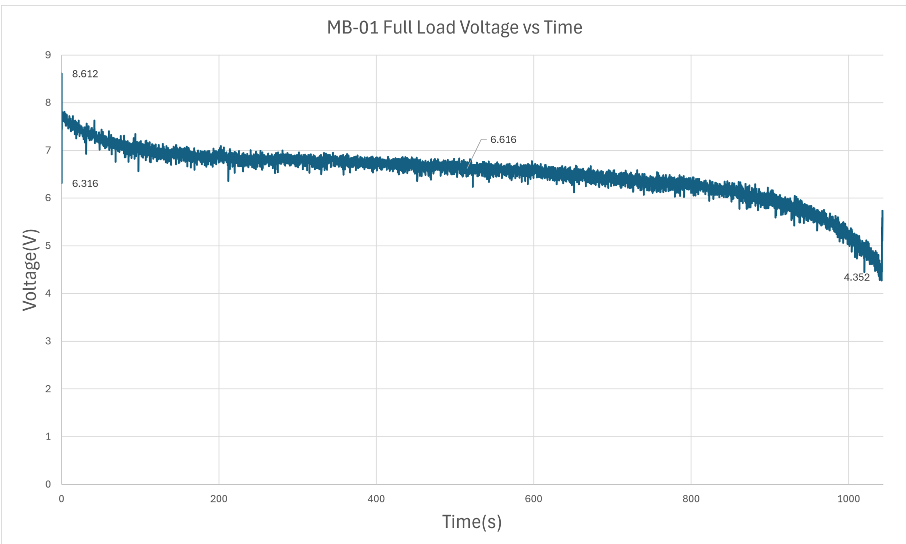

Figure 4.4: MB-01 Raw Full Load Voltage

Figure 4.5: MB-01 Smoothed Full Load Voltage

The raw voltage signal in Figure 4.4 contained continuous fluctuations throughout the discharge process, caused by the transient voltage drops and overshoots resulting from the high-frequency switching current behaviour described in the previous section. Despite this, the smoothed voltage trend in Figure 4.5 followed the characteristic discharge behaviour of a NiMH battery under constant current loading from Figure 4.1, further supporting the observation that the drivetrain operation was dominated by a relatively stable average current demand.

Near the end of the full-load test, a sudden voltage rise is visible in Figure 4.4, following the stoppage of the steering servo, which was taken as the end of normal operation and therefore the termination point of the test.

4.1.1.3 Power Behaviour

Figures 4.6 and 4.7 show the power loading behaviour of the MB-01 platform throughout the sustained full-load endurance test. The raw power signal is presented alongside a smoothed trend obtained by applying a moving average filter to better illustrate the underlying sustained power demand.

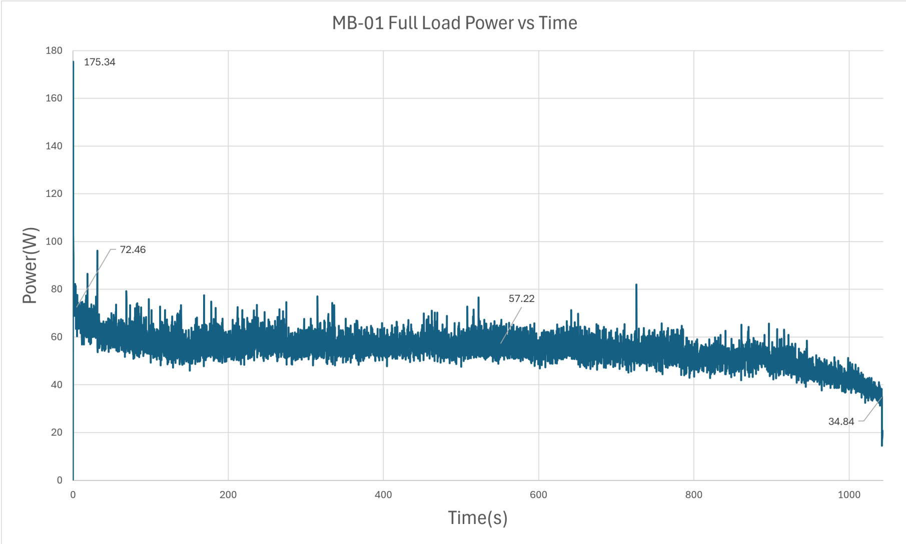

Figure 4.6: MB-01 Raw Full Load Power

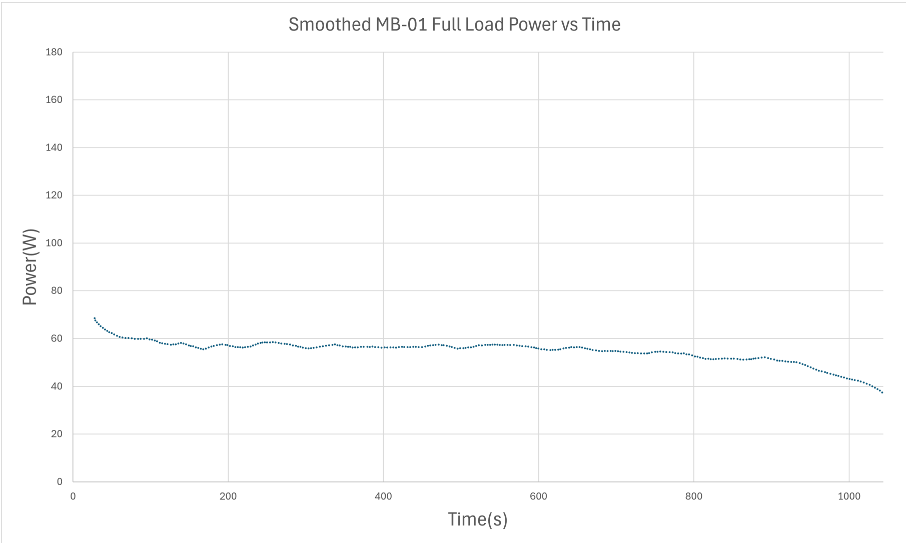

Figure 4.7: MB-01 Smoothed Full Load Power

A very high initial transient power peak of approximately 175.3 W is visible as a sharp spike at the start of the raw power signal in Figure 4.6, resulting from the high startup current demand at maximum battery voltage during acceleration from rest. Following this initial peak, the smoothed power trend in Figure 4.7 generally followed the same declining trend as the voltage curve from Figure 4.5. The fact that the power trend closely followed the voltage trend provides further evidence that the average drivetrain current remained approximately constant throughout operation, consistent with the observations made in the current behaviour section.

Similar to the current behaviour, the raw power readings also contained continuous fluctuations throughout operation, caused by the combined effect of the switching current behaviour and the corresponding transient voltage drops described in the previous sections.

4.1.2 TT-02

4.1.2.1 Current Behaviour

Figures 4.8 and 4.9 show the measured current behaviour of the TT-02 platform during the sustained full-load endurance test. The raw current signal is presented alongside a smoothed trend obtained by applying a moving average filter, in order to separate the underlying average drivetrain current demand from the high-frequency switching fluctuations introduced by the ESC.

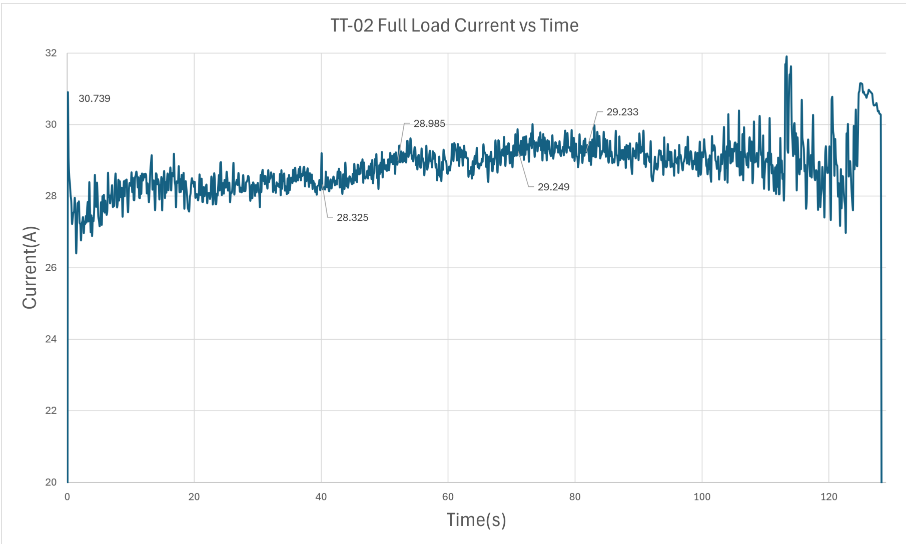

Figure 4.8: TT-02 Raw Full Load Current

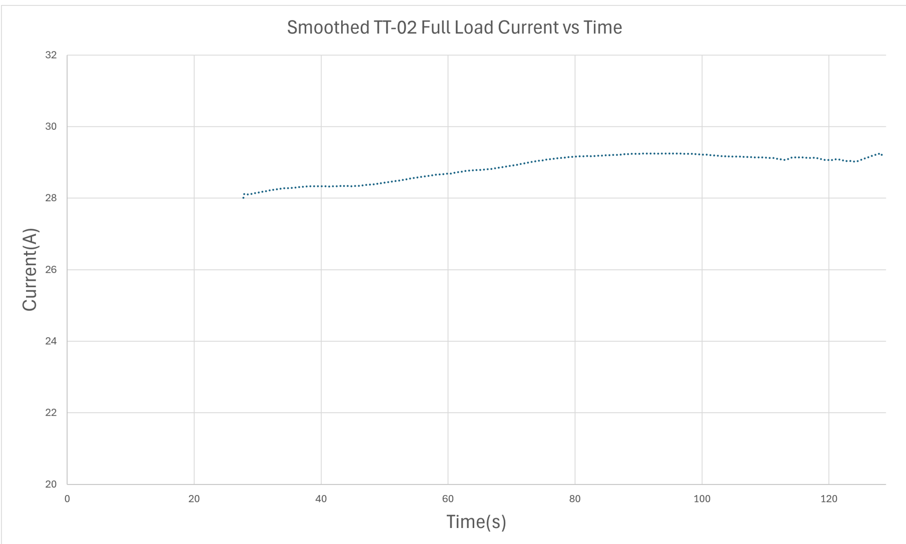

Figure 4.9: TT-02 Smoothed Full Load Current

Similar to the MB-01 platform, an initial transient current peak of approximately 30.7 A is visible as a sharp spike at the start of the raw current signal in Figure 4.8, occurring during acceleration from rest. The raw current signal contained continuous switching ripple between approximately 27–31 A throughout operation with a logging interval of approximately 110 ms.

The TT-02 smoothed current in Figure 4.9 showed a gradual increase in average current demand during the initial phase of the discharge, rising from approximately 28.1 A to 29.2 A before stabilising into a relatively uniform plateau for the remainder of the test. This behaviour is consistent with the drivetrain initially compensating for the significantly increased voltage drop across the internal resistance of the battery pack under the substantially higher sustained current demand of the TT-02 drivetrain, until a steady operating point was reached. However, it is also worth noting that the gradual rise in average current observed during the initial phase of the discharge was particularly prominent in the TT-02 results due to the comparatively rapid discharge of the low-capacity battery pack under the substantially higher sustained current demand. Had the battery capacity been larger, the drivetrain would have had sufficient time to reach and sustain a stable operating point for a longer period, and the overall current trend would likely have appeared considerably constant over a larger timescale, more consistent with the behaviour observed in the MB-01 platform.

Some unstable behaviour was observed near the end of the test from approximately $t \approx 110s$ onwards, visible as increasingly erratic fluctuations in the raw current signal in Figure 4.8. In the case of the MB-01 platform, the comparatively lower sustained current demand resulted in less severe voltage drop across the internal resistance of the battery pack, allowing the drivetrain to remain comparatively stable even near the lower operating voltage region. However, in the case of the TT-02 platform, the substantially higher sustained current demand resulted in significantly larger voltage drop during operation. As the battery voltage decreased near the end of discharge, the combined effect of the severe voltage drop together with the continuous ESC-induced current fluctuations resulted in increasingly unstable drivetrain behaviour. This region is therefore considered outside the normal sustained operating behaviour of the platform.

4.1.2.2 Voltage Behaviour

Figures 4.10 and 4.11 show the voltage behaviour of the MB-01 platform battery throughout the sustained full-load endurance test. The raw voltage signal is presented alongside a smoothed trend obtained by applying a moving average filter to better illustrate the underlying battery discharge behaviour.

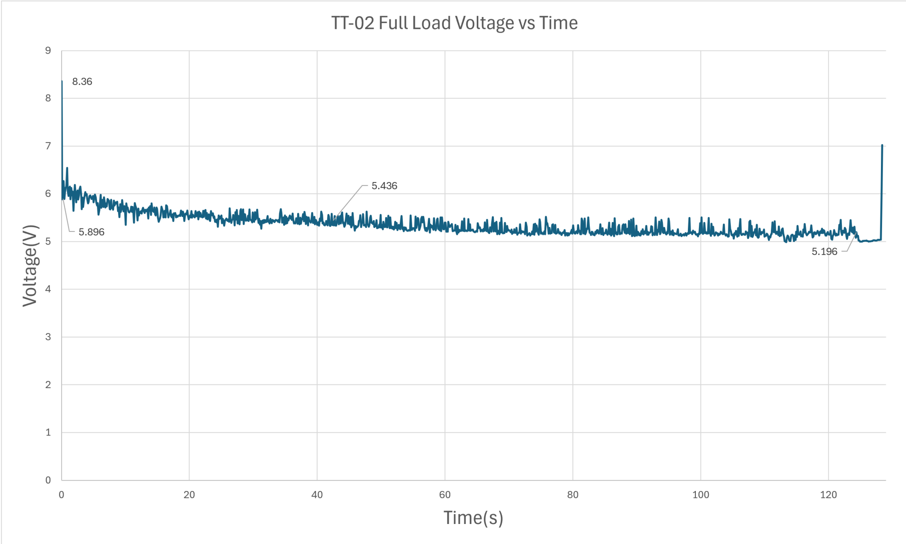

Figure 4.10: TT-02 Raw Full Load Voltage

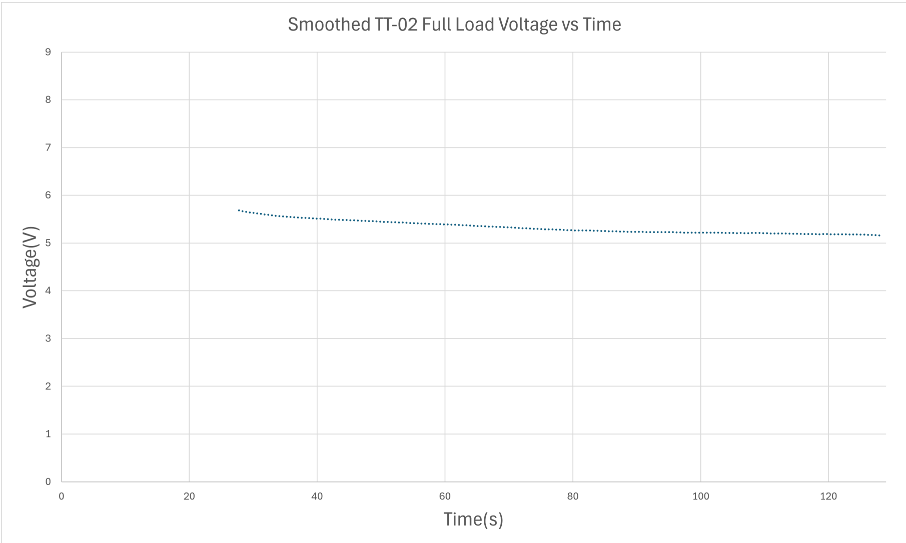

Figure 4.11: TT-02 Smoothed Full Load Voltage

A steep initial voltage drop from approximately 8.36 V down to around 5.9 V is visible at the start of the raw voltage signal in Figure 4.10, resulting from the immediate large current demand of the platform. The raw voltage signal also contained continuous fluctuations throughout operation, caused by the transient voltage drops and overshoots resulting from the high-frequency switching current behaviour described in the current behaviour section.

Compared to the MB-01 full-load voltage behaviour, the smoothed voltage trend of the TT-02 platform from Figure 4.11 appears considerably flatter and more linear. This can be attributed to two contributing factors. Compared to the MB-01 platform, the TT-02 drivetrain operated under substantially higher sustained current demand, resulting in a significantly larger voltage drop across the internal resistance of the battery pack throughout operation. As a result, the battery voltage was already operating within a very compressed voltage range of approximately 5.2–5.9 V for most of the discharge process, compared to the wider operating range observed in the MB-01 platform. Consequently, the smoothed voltage trend appears flatter. Additionally, it can be seen in Figure 4.1 that as the C-rate increases, the characteristic NiMH constant-current discharge voltage plateau becomes progressively less defined, and the curve appears increasingly linear. At the substantially higher sustained current demands of the TT-02 platform, the characteristic plateau region of the discharge curve would therefore be expected to be significantly less prominent, and consequently, the smoothed voltage trend appears more linear. This suggests the voltage behaviour of the TT-02 platform is still consistent with the characteristic behaviour of a NiMH battery under constant current discharge, simply observed under conditions of substantially higher current demand and a more compressed operating window.

4.1.2.3 Power Behaviour

Figures 4.12 and 4.13 shows the power loading behaviour of the TT-02 platform throughout the sustained full-load endurance test. The raw power signal is presented alongside a smoothed trend obtained by applying a moving average filter to better illustrate the underlying sustained power demand.

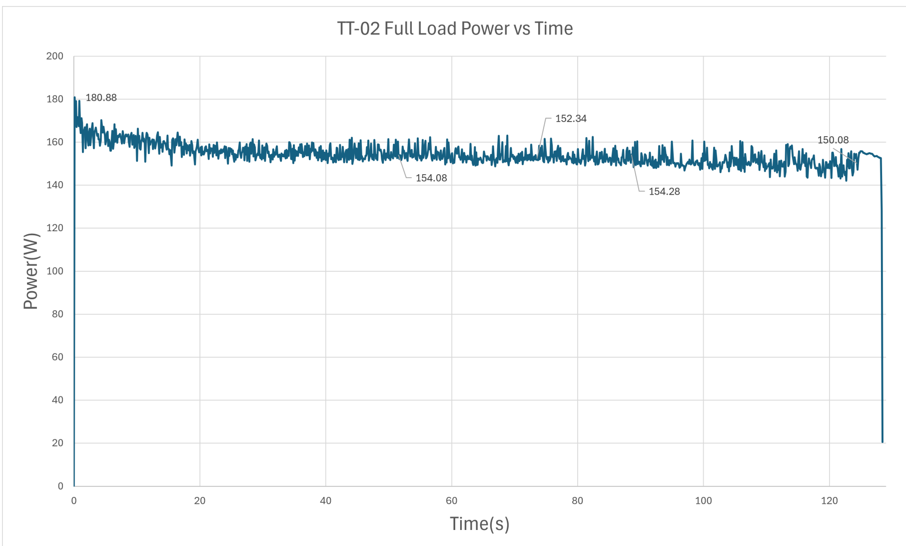

Figure 4.12: TT-02 Raw Full Load Power

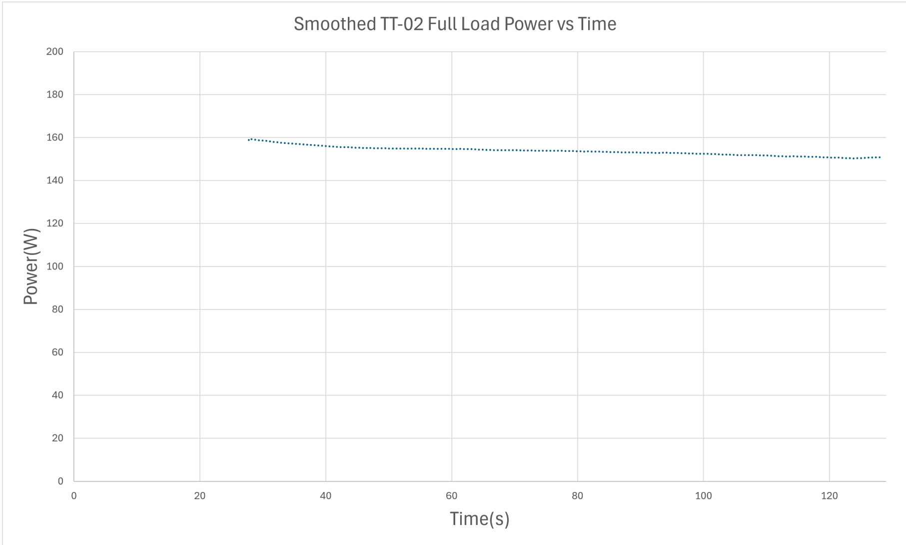

Figure 4.13: TT-02 Smoothed Full Load Power

An initial transient power peak of approximately 180.9 W is visible as a sharp spike at the start of the raw power signal in Figure 4.12, resulting from the large startup current demand at maximum battery voltage during acceleration from rest.

Similar to the MB-01 platform, the smoothed power trend in Figure 4.13 for the TT-02 platform also generally followed the same declining trend as the voltage curve throughout the discharge process, declining gradually from approximately 159 W to around 150 W. Although a gradual rise in average current was observed in the current behaviour section, the fact that the power trend mirrors the voltage trend suggests that the variation in current was relatively and sufficiently small, and the overall current demand can be reasonably approximated as constant throughout the discharge process, consistent with the observations made in the current behaviour section.

Similar to the current behaviour, the raw power readings also contained continuous fluctuations throughout operation, caused by the combined effect of the switching current behaviour and the corresponding transient voltage drops described in the previous sections.

4.2 Raw Drive Cycles

Figures 4.14 and 4.15 show the representative measured drive-cycle current profiles obtained for the MB-01 and TT-02 platforms respectively.

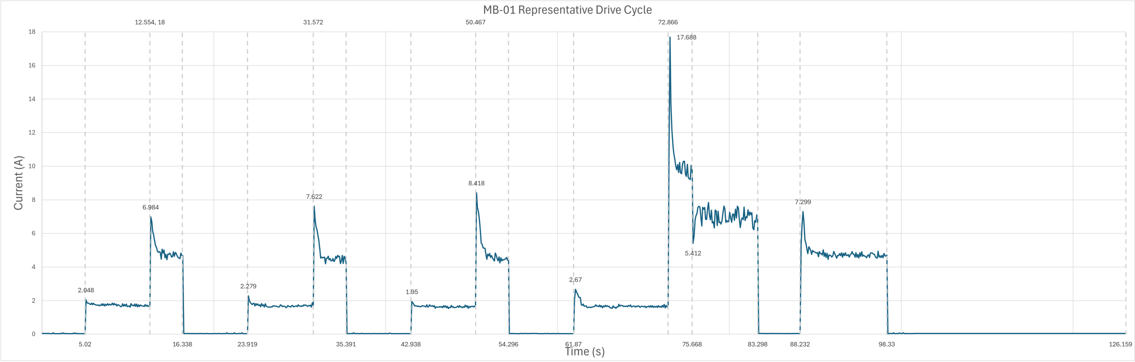

Figure 4.14: Raw MB-01 Drive Cycle

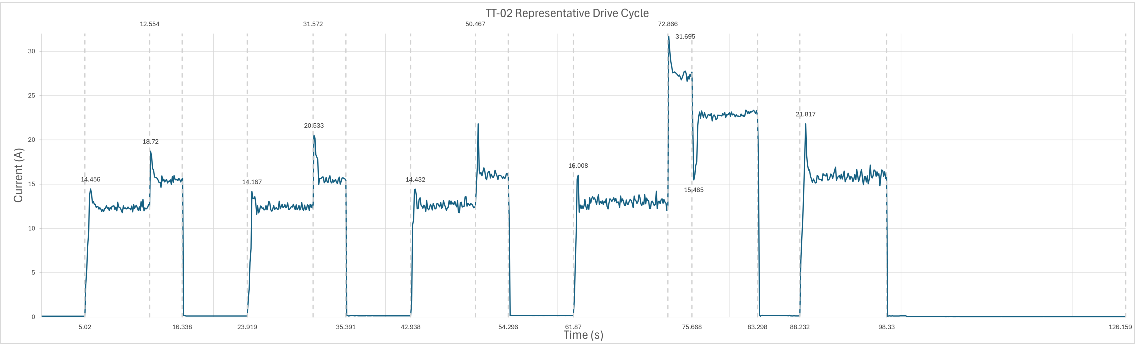

Figure 4.15: Raw TT-02 Drive Cycle

The overall structure of both profiles is consistent with the stepped loading pattern of the SFUDS drive cycle. The total duration of approximately 126 seconds, as well as the durations of each operating region, are consistent with the scaled SFUDS cycle time scale derived using the scaling factor of $\sqrt{1/10}$ applied to the original 400-second SFUDS profile.

Minor variations were observed between the sustained loading levels of the operating regions of the reproduced drive-cycles that are defined as identical loading levels in the original SFUDS cycle, as can be seen by comparing Figure 3.2 with Figures 4.14 and 4.15. These variations are attributable to the inherent variability of manual vehicle operation. Despite this, the overall loading sequence and structure of the profiles remained consistent with the intended SFUDS-representative pattern.

Both profiles exhibited clearly observable transient startup current peaks during acceleration events, followed by comparatively gradual settling toward sustained average current demand regions. Similarly, sudden current drops were observed during braking and coasting transitions, after which the drivetrain current gradually stabilised toward the corresponding lower operating region. Despite the application of calibration adjustments in data acquisition, noticeable current fluctuations remained visible throughout both profiles, indicating that the fluctuations originated predominantly from the actual drivetrain and ESC switching behaviour rather than measurement noise alone.

Comparing the two platforms, the MB-01 profile exhibited comparatively moderate loading behaviour, with low sustained current demands and a maximum transient acceleration peak reaching 17.69 A. The TT-02 platform demonstrated substantially more aggressive loading behaviour across all equivalent operating regions, with significantly higher sustained current demands and a maximum transient acceleration peak reaching 31.69 A. These measured profiles provided the basis for the development of the sequenced representative drive cycles presented in Section 4.3.

4.3 Sequenced Drive Cycles

Figures 4.16 and 4.17 show the sequenced representative drive-cycle profiles derived from the experimentally reproduced scaled SFUDS drive cycles for both platforms, obtained by simplifying the raw measured current profiles into discrete constant-current segments, as described in Section 3.3.2. These sequenced profiles represent the final SFUDS-representative drive cycles developed in this work.

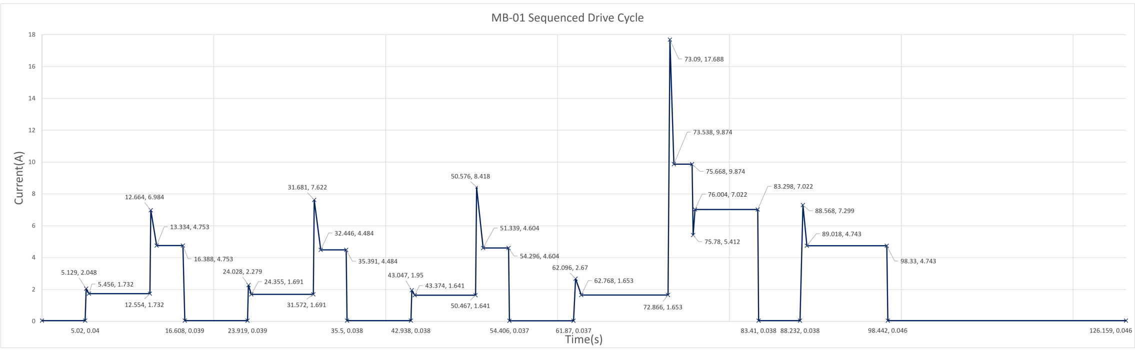

Figure 4.16: Sequenced MB-01 Representative Drive Cycle

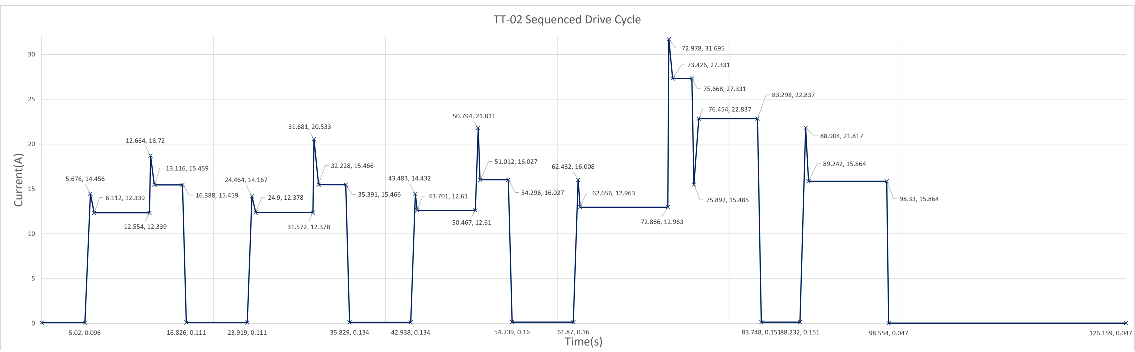

Figure 4.17: Sequenced TT-02 Representative Drive Cycle

For the MB-01 platform, the lowest sustained operating regions — corresponding to the minimum load required for the platform to move — show a current demand of approximately 1.64–1.73 A, while the most demanding operating region — corresponding to maximum throttle — settled to a sustained level of approximately 9.87 A. The specific values for each operating region are indicated directly on Figure 4.16. For the TT-02 platform, the loading profile shows substantially higher current levels across all equivalent operating regions, with the lowest sustained regions showing approximately 12.34–12.61 A and the most demanding region settling to a sustained level of approximately 27.33 A. The specific values for each operating region are indicated directly on Figure 4.17.

4.4 Drive Cycle Replay

The generated sequenced drive-cycle profiles were replayed on the same NiMH battery packs used during the experimental drive-cycle measurements, using the EA Elektro-Automatik EL 9080-45 T programmable electronic load test bench, with continuous monitoring throughout the replay using the ETC developed in this thesis. Figures 4.18 and 4.19 show the current profiles recorded by the ETC during the replay experiment for both platforms.

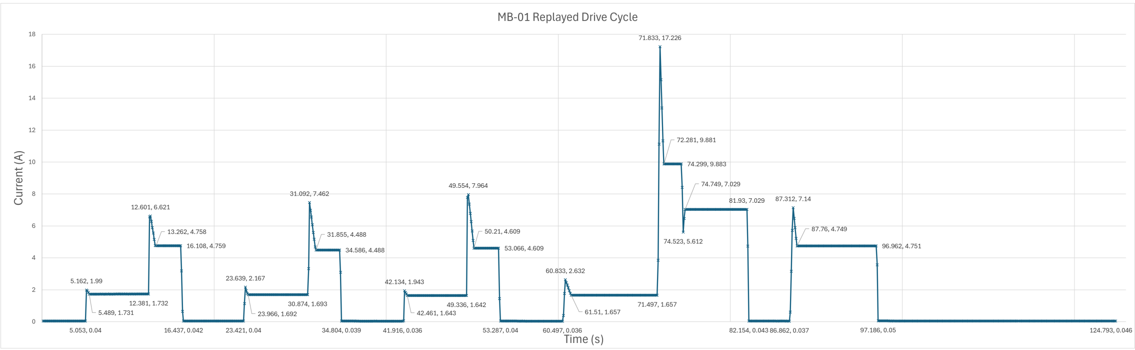

Figure 4.18: MB-01 Replayed Drive Cycle

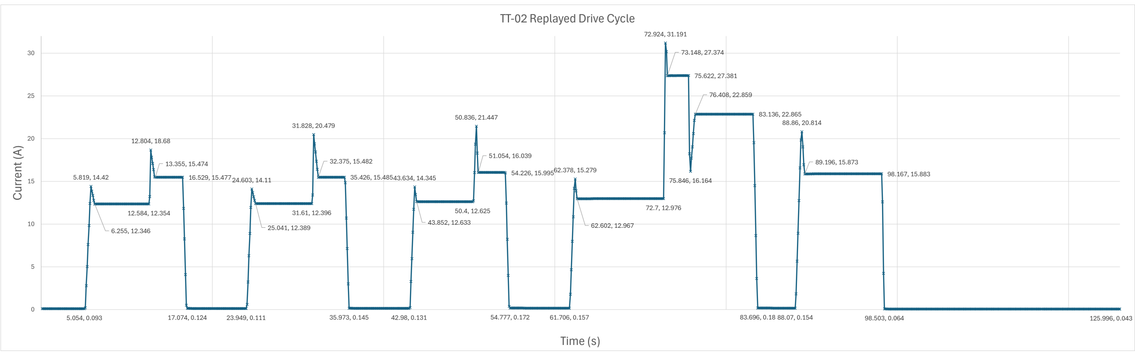

Figure 4.19: TT-02 Replayed Drive Cycle

On comparing the replayed profiles in Figures 4.18 and 4.19 with the sequenced representative drive cycle profiles in Figures 4.16 and 4.17, the replayed profiles closely match the derived drive cycle profiles in terms of loading pattern, current levels and time scale. This demonstrates that the derived drive cycles are reproducible under controlled laboratory conditions and validates the test bench as a practical means of subjecting future structural battery prototypes to representative SFUDS-based drive cycle loading without requiring direct integration into the RC vehicle platforms.

Notably, the current profiles recorded during replay are devoid of the high-frequency fluctuations observed in the raw current signals measured during direct vehicle operation, despite being recorded using the same ETC. This confirms that the fluctuations present in the original raw vehicle measurements originated predominantly from the ESC switching behaviour of the RC powertrains rather than from measurement noise.

5

Discussion

5.1 Interpretation of Results

The full-load endurance testing conducted in this work demonstrated that the electrical loading behaviour of both RC vehicle platforms is primarily characterized by current demand, evidenced by the comparatively stable average current demand observed throughout sustained operation on both platforms, with the battery voltage declining throughout discharge while the current remained approximately constant. This observation directly supported the decision to develop the representative drive cycles in terms of current rather than power, as discussed in Section 3.3.2.

The substantially higher loading demands of the TT-02 platform across all operating regions reflect the more powerful drivetrain configuration of this platform, and indicate that the electrical requirements imposed on a structural battery intended for higher-performance small-scale mobility applications would be significantly more demanding than those for a lower-performance platform such as the MB-01. These differences have direct implications for structural battery prototype development. For early-stage development, the MB-01 platform represents a more suitable and accessible initial target for assessing the feasibility of structural batteries as a concept, as the comparatively lower sustained loading demands impose less severe electrochemical and thermal requirements on the battery system, providing a more realistic initial benchmark for feasibility evaluation. The TT-02 platform represents a considerably more challenging target, more appropriate for later-stage evaluation once basic feasibility of structural battery systems has been demonstrated. With high-performance mobility systems considered as a potential future application for structural batteries, testing feasibility at a high-performance small-scale application like the TT-02 platform can be a suitable first step in later-stage development. It should be noted that both platforms were characterized in this work to establish representative loading requirements across different performance levels, providing a broader basis for future structural battery development rather than targeting a single application.

The representative drive cycle profiles serve a dual purpose — establishing the representative electrical loading requirements that structural battery prototypes for each platform would need to satisfy, while simultaneously providing SFUDS-representative drive cycles that can be directly used for laboratory-based battery prototype testing. The constant-current discharge characteristics of these platforms, and consequently the derived drive cycles, indicate that the primary electrochemical requirement imposed on a structural battery prototype for these applications is the ability to sustain a stable discharge current throughout the operational period, rather than maintaining constant power output. The transient current peaks and drops represent an additional requirement, indicating that structural battery prototypes for these platforms would need sufficient transient response capability to tolerate instantaneous current demands significantly exceeding the sustained operating level.

5.2 Methodology Evaluation

The overall methodology developed in this work provided a practical approach for generating representative drive cycle profiles from experimental scaled vehicle operation and reproducing them under controlled laboratory conditions. The methodology was verified through the close agreement between the replayed profiles and the intended sequenced drive cycle profiles in terms of loading pattern, current levels, and time scale, as demonstrated in Section 4.4.

The drive cycles were reproduced through manual throttle operation, which was the most practical means of capturing genuine transient drivetrain behaviour through actual vehicle operation. However, it should be acknowledged that this introduced inherent variability in the loading levels between nominally identical operating regions. An automated throttle control system would reduce this variability and improve the consistency of the reproduced profiles, particularly for the operating regions defined at identical loading levels in the original SFUDS cycle. However, implementing such a system was considered beyond the scope of this work, as the primary objective was to capture representative drivetrain loading behaviour through actual vehicle operation rather than to achieve precise repeatability in the throttle input.

The time scaling approach adopted in this work assumed that vehicle dynamics parameters scaled proportionally between scales, allowing a simple kinematic scaling factor to be applied to derive the scaled SFUDS time base. A more rigorous approach to determine the dynamic parameter ratios, analogous to those described in [10], would provide a more physically accurate basis for the scaled drive cycle time base. However, such an approach would have required significant dynamic analysis of the RC vehicle platforms, which was outside the scope of this work, given that the primary objective was to develop loading profiles for the small-scale RC platforms rather than to achieve precise dynamic similarity between scales.

The methodology developed in this thesis can be considered transferable to other applications, since the core process — scaling a reference drive cycle, experimentally characterizing the drivetrain loading behaviour, simplifying the measured profiles into sequenced profiles, and replaying them on a test bench — remains applicable beyond the RC vehicle platforms used in this work. For transferring the methodology to larger-scale prototype evaluation, the scaling factor derived in this work would need to be re-derived for the target platform, and whether a single kinematic scaling factor remains a valid and sufficient means of scaling the drive cycle at a larger scale would need to be critically assessed. Beyond the scaling factor, however, the core methodology for generating and testing the drive cycles would remain the same. For transferring the methodology to platforms other than these RC platforms, the load characterization of the new platform would need to be repeated, as the approximately constant current behaviour observed for the RC vehicle platforms in this work may not hold for other drivetrain configurations. The outcome of this characterization would then determine whether the drive cycle profiles should be developed in terms of current or power, and the sequencing and replay approach would follow accordingly.

5.3 Limitations and Future Work

The RC vehicle-based methodology developed in this thesis does not fully replicate the scaled electrical and mechanical behaviour of full-scale EVs. This was considered acceptable given that the primary objective was to characterize the representative loading conditions of small-scale platforms relevant to early structural battery prototype development, rather than to achieve complete dynamic similitude with full-scale vehicle operation. As structural battery technology matures, extending the methodology by modifying the platforms with more rigorous dynamic similitude analysis [10] would provide increasingly representative scaled loading profiles.

Regenerative braking was not incorporated in the drive cycles developed in this work, as the RC vehicle platforms used were not equipped with regenerative braking capability. As a result, the reproduced drive cycles represent driving-only loading conditions, with the regenerative charging events present in the original SFUDS profile excluded. For future work, identifying platforms capable of regenerative braking and incorporating regenerative events into the drive cycle profiles would provide a more complete representation of realistic EV operation, and would additionally allow the transient charge acceptance capability of structural battery prototypes to be evaluated — an increasingly relevant characteristic given the prominence of regenerative braking in modern EV drivetrains.

Structural battery prototypes were not available within the timeframe of this work. The most important direction for future work is therefore to apply the developed drive cycles to actual structural battery prototypes developed for these applications, evaluating their sustained loading tolerance, transient response capability, thermal behaviour, and long-term cycling performance under the representative loading conditions established in this work.

Finally, the drive cycles developed in this work are based on a simplified drive cycle like the SFUDS profile, which was considered appropriate for early-stage prototype evaluation. For more advanced prototype evaluation, developing equivalent drive cycles based on complex drive cycles like the FUDS profile would provide a more comprehensive representation of realistic driving conditions.

6
Conclusion

This work established representative electrical loading profiles and a laboratory replay methodology for small-scale mobility applications, intended to support future structural battery prototype development and evaluation. Using 1:10 scale RC vehicle platforms, the dynamic electrical loading behaviour of two drivetrain configurations representing different performance levels was characterized under both sustained and dynamic operating conditions by deriving representative SFUDS-based drive cycles from experimental vehicle operation. The developed drive cycles established representative operating conditions, transient response behaviour, and approximate electrical loading requirements that future structural battery prototypes intended for similar-scale applications would need to satisfy during practical operation.

The MB-01 platform was identified as the most suitable initial target for early-stage structural battery prototype development due to its comparatively lower loading demands, and the results of this work provide a basis for estimating the minimum electrical requirements that the earliest structural battery prototypes would need to satisfy to operate this platform at all. Since the electrical loading behaviour of the platforms is primarily characterized by current demand, voltage is not the defining parameter for the prototypes. The prototypes only need to maintain a sufficient terminal voltage to keep the platform operational — approximated by the full-load test termination voltage of approximately 4.4 V — while delivering the required current demand. The lowest sustained operating region of the MB-01 drive cycle, corresponding to the minimum load required for the platform to move at all, shows a sustained current demand of approximately 1.64–1.73 A, with a maximum initial instantaneous peak of approximately 2.28 A. These voltage and current requirements represent the minimum electrical requirements for a structural battery prototype to operate the MB-01 platform at all, and could serve as the most basic initial target for demonstrating the feasibility of structural batteries in a small-scale mobility application.

The laboratory replay methodology developed alongside the drive cycles was also validated, demonstrating that future structural battery prototypes can be subjected to representative drivetrain loading conditions under controlled laboratory conditions without requiring direct vehicle integration. The three specific objectives of this work were thereby fulfilled — the electrical loading behaviour of the RC vehicle platforms was characterized, representative drive cycle profiles were derived, and a laboratory replay methodology was established, providing a practical and transferable foundation for experimental evaluation of future structural battery prototypes.

References

[1] Tamiya Global . Mini Cooper MB-01 RC Platform; 2026. Available from: https://www.tamiya.com/english/products/58747/index.html.

[2] Tamiya Global. McLaren Senna TT-02 RC Platform; 2026. Available from: https://www.tamiya.com/english/products/58711/index.html.

[3] Texas Instruments. INA219 Current/Power Monitor Datasheet; 2026. Available from: https://www.ti.com/lit/ds/symlink/ina219.pdf.

[4] Brandt DD. Driving Cycle Testing of Electric Vehicle Batteries and Systems. Journal of Power Sources. 1992;40(1):73-9. Available from: https://pdf.sciencedirectassets.com/271367/1-s2.0-S0378775300X01024/1-s2.0-037877539280039E.

[5] Hu WK, Geng MM, Gao XP, Burchardt T, Gong ZX, Noréus D, et al. Effect of Long-Term Overcharge and Operated Temperature on Performance of Rechargeable NiMH Cells. Journal of Power Sources. 2006;159(2):1478-83. Available from: https://www.researchgate.net/publication/223211274_Effect_of_long-term_overcharge_and_operated_temperature_on_performance_of_rechargeable_NiMH_cells.

[6] Asp L, Greenhalgh ES. Structural Batteries: A Review. Molecules. 2021;26(8):2203. Available from: https://pmc.ncbi.nlm.nih.gov/articles/PMC8068925/pdf/molecules-26-02203.pdf.

[7] Kühnelt H, Beutl A, Mastropierro F, Laurin F, Willrodt S, Bismarck A, et al. Structural Batteries for Aeronautic Applications—State of the Art, Research Gaps and Technology Development Needs. Aerospace. 2022;9(1):7. Available from: https://www.mdpi.com/2226-4310/9/1/7.

[8] Asp L. Multifunctional Composite Materials for Structural Energy Storage. Chalmers University of Technology. 2023. Available from: https://research.chalmers.se/publication/536416/file/536416_Fulltext.pdf.

[9] Chaudhary R, Xu J, Xia Z, Asp LE. Unveiling the Multifunctional Carbon Fiber Structural Battery. Advanced Materials. 2024;36(48):e2409725. Available from: https://advanced.onlinelibrary.wiley.com/doi/10.1002/adma.202409725.

[10] Kumari S, K AR, Mukhopadhyay S, Hota AR. Development of a Scaled Setup for Experimental Study of the Effect of Lateral Dynamics on Energy Consumption in Electric Vehicles. 2025 IEEE/AIAA Transportation Electrification Conference and Electric Aircraft Technologies Symposium (ITEC+EATS). 2025:1-5. Available from: https://ieeexplore.ieee.org/stamp/stamp.jsp?tp=&arnumber=11098029.

[11] JOY-iT. NodeMCU ESP32 Microcontroller Development Board Datasheet; 2023. Available from: https://joy-it.net/files/files/Produkte/SBC-NodeMCU-ESP32/SBC-NodeMCU-ESP32_Datasheet_2023-09-13.pdf.

[12] Panchal S, Mathew M, Dincer I, Agelin-Chaab M, Fraser R, Fowler M. Thermal and Electrical Performance Assessments of Lithium-Ion Battery Modules for an Electric Vehicle Under Actual Drive Cycles. Electric Power Systems Research. 2018;163(1):18-27. Available from: https://www.sciencedirect.com/science/article/pii/S0378779618301585?via%3Dihub.

[13] Sisk B, Hallac P, Zhang Q, Zhang Z. Connecting Vehicle Requirements with Battery Design and Testing: Linking Drive Cycles with Material Properties. SAE Technical Paper Series. 2013. Available from: https://www.researchgate.net/publication/289576454_Connecting_Vehicle_Requirements_with_Battery_Design_and_Testing_Linking_Drive_Cycles_with_Material_Properties.

[14] Electric Vehicle Battery Test Procedures Manual; 1996. Available from: https://www.osti.gov/servlets/purl/214312.

[15] Bae SHS. Realistic Drive Cycle-Based Testing Methodology for Batteries in Micro Hybrid Electric Vehicles. Journal of Electrical Engineering and Technology. 2024;1(1):0-12. Available from: https://link.springer.com/article/10.1007/s42835-024-02101-5.

[16] Cole GH. A Simplified Battery Discharge Profile Based Upon the Federal Urban Driving Schedule. Idaho National Engineering Laboratory. 1989;1(1):0-9. Available from: https://www.osti.gov/servlets/purl/5380770.

[17] L H Saw / K Somasundaram / Y Ye AAOT. Electro-thermal analysis of Lithium Iron Phosphate battery for electric vehicles. Journal of Power Sources. 2013;1(1):0-8. Available from: https://www.sciencedirect.com/science/article/pii/S0378775313017059.

[18] Redey L. Dynamic-Performance Measurements of Battery Cells for Electric Vehicle and Other Applications. Argonne National Laboratory. 1984;(ANL/CNSV-TM-161). Available from: https://www.osti.gov/servlets/purl/5244124.

[19] Hollenkamp AF, Lam LT, Phyland CG, Wilson NC. Evaluation of Lead-/Acid Batteries Under Simulated Electric-Vehicle Duty: Development of Design Parameters on the Basis of SFUDS Performance. Journal of Power

Sources. 1996;59(2):177-83. Available from: https://www.sciencedirect.com/science/article/pii/0378775395023208.

[20] Tektronix. Programmable Electronic DC Load Datasheet; 2026. Available from: https://www.farnell.com/datasheets/2197578.pdf.

[21] Tektronix. Programmable Electronic DC Load User Manual; 2026. Available from: https://download.tek.com/manual/33210511_EN.pdf.

A

Appendix

A.1 Sensor Calibration for 32A 16V

```
void Adafruit_INA219::setCalibration_16V_32A()
{
  // For 16V bus, 0.01 ohm shunt, up to about 32A

  ina219_calValue = 4096;
  ina219_currentDivider_mA = 1;    // 1 mA per bit
  ina219_powerMultiplier_mW = 20; // 20 mW per bit

  Adafruit_BusIO_Register calibration_reg =
    Adafruit_BusIO_Register(i2c_dev, INA219_REG_CALIBRATION,
      2, MSBFIRST);
  calibration_reg.write(ina219_calValue, 2);

  uint16_t config = INA219_CONFIG_BVOLTAGERANGE_16V |
                    INA219_CONFIG_GAIN_8_320MV |
                    INA219_CONFIG_BADCRES_12BIT |
                    INA219_CONFIG_SADCRES_12BIT_32S_17MS |
                    INA219_CONFIG_MODE_SANDBVOLT_CONTINUOUS;

  Adafruit_BusIO_Register config_reg =
      Adafruit_BusIO_Register(i2c_dev, INA219_REG_CONFIG,
      2, MSBFIRST);
  _success = config_reg.write(config, 2);
}
/*!
 *  @brief  Provides the the underlying return value from the
 *           last operation called on the device.
 *  @return true: Last operation was successful false:
            Last operation failed
 *  @note   For function calls that have intermediary
 *           device operations, e.g. calibration before
 */
bool Adafruit_INA219::success() { return _success; }
```

A.2 Sensor Sample Time Calibration

```
/** mask for shunt ADC resolution bits **/
#define INA219_CONFIG_SADCRES_MASK (0x0078)
// Shunt ADC Resolution and Averaging Mask

/** values for shunt ADC resolution **/
enum {
  INA219_CONFIG_SADCRES_9BIT_1S_84US = (0x0000),
  // 1 x 9-bit shunt sample
  INA219_CONFIG_SADCRES_10BIT_1S_148US = (0x0008),
  // 1 x 10-bit shunt sample
  INA219_CONFIG_SADCRES_11BIT_1S_276US = (0x0010),
  // 1 x 11-bit shunt sample
  INA219_CONFIG_SADCRES_12BIT_1S_532US = (0x0018),
  // 1 x 12-bit shunt sample
  INA219_CONFIG_SADCRES_12BIT_2S_1060US =
      (0x0048), // 2 x 12-bit shunt samples averaged
      together
  INA219_CONFIG_SADCRES_12BIT_4S_2130US =
      (0x0050), // 4 x 12-bit shunt samples averaged
      together
  INA219_CONFIG_SADCRES_12BIT_8S_4260US =
      (0x0058), // 8 x 12-bit shunt samples averaged
      together
  INA219_CONFIG_SADCRES_12BIT_16S_8MS =
      (0x0060), // 16 x 12-bit shunt samples averaged
      together
  INA219_CONFIG_SADCRES_12BIT_32S_17MS =
      (0x0068), // 32 x 12-bit shunt samples averaged
      together
  INA219_CONFIG_SADCRES_12BIT_64S_34MS =
      (0x0070), // 64 x 12-bit shunt samples averaged
      together
  INA219_CONFIG_SADCRES_12BIT_128S_69MS =
      (0x0078), // 128 x 12-bit shunt samples averaged
      together
      };
```

A.3 Source Code

```
/* ESP32 nodeMCU with Adafruit INA219
   Measure current, voltage and power via I2C
*/

#include <Wire.h>
#include <Adafruit_INA219.h>
#include <SD.h>
#include <SPI.h>

// Default I2C address for INA219 is 0x40
//(can be changed via A0/A1 jumpers: 0x41, 0x44, 0x45)
//#define INA219_ADDRESS 0x40

// SD card CS pin VSPI (VSPI default CS = GPIO5)
#define SD_CS_PIN 5
#define LED_PIN 2

// Create INA219 object
Adafruit_INA219 ina219 = Adafruit_INA219(0x40);
File dataFile;

unsigned long readingCount = 0;
bool sdCardReady = false;
bool ledBlinking = false;
bool checkSDCard() {
  // Quick check: try to open root directory
  File root = SD.open("/");
  if (root) {
    root.close();
    return true;
  }
  return false;
}

void setup() {
  Serial.begin(115200);
  while (!Serial) { delay(10); }

  Serial.println("INA219 test with ESP32 nodeMCU
  and Data storing in SD card");

  // Initialize LED blink
  pinMode(LED_PIN, OUTPUT);
```

```
  digitalWrite(LED_PIN, LOW);

  // Initialize I2C
  Wire.begin(21, 22);

  // Initialize INA219 to specific address
  if (!ina219.begin(&Wire)) {
    Serial.println("Couldn't find INA219 chip! ");
    while (1) {
      delay(10);
    }
  }

  Serial.println("Found INA219 chip!");

  // Configure INA219 for better accuracy
  // Set calibration for 16V 32A range (default)
  // Options: setCalibration_32V_2A(),
  // setCalibration_32V_1A(),
  // setCalibration_16V_400mA()
  ina219.setCalibration_16V_32A();

  // Initialize SPI for SD card
  SPI.begin(18, 19, 23, SD_CS_PIN);

  Serial.print("Initialize the SD Card \n");

  if (!SD.begin(SD_CS_PIN)) {
    Serial.println("Failed! check wiring");
    Serial.println("Continuing without SD card");
    sdCardReady = false;
  } else {
    Serial.println("SUCCESS");
    sdCardReady = true;

    // Create CSV FILE
    if (!SD.exists("/datalog.csv")) {
      dataFile = SD.open("/datalog.csv", FILE_WRITE);
      if (dataFile) {
        dataFile.println("Reading,Timestamp_ms,
        Current_A,Voltage_V,Power_W");
        dataFile.close();
        Serial.println("Created datalog.csv with headers");
      }
    } else {
      Serial.println("Using existing datalog.csv");
```

```
    }
  }

  Serial.println("Setup complete!\n");
}

void loop() {

  // Auto-detect SD card reinsertion
  if (!sdCardReady && checkSDCard()) {
    if (SD.begin(SD_CS_PIN)) {
      sdCardReady = true;
      Serial.println("-> SD card reinserted!
      Logging resumed.");
    }
  }

  // Read measurement
  float current_mA = ina219.getCurrent_mA();
  float voltage_V = ina219.getBusVoltage_V();
  float power_mW = ina219.getPower_mW();
  unsigned long timestamp = millis();
  readingCount++;

  // INA219 returns: current in mA, voltage in V,
  // power in mW
  float current_A = current_mA / 1000.0;
  float Power_W = power_mW / 1000.0;

  // Read measurement
  if (voltage_V <= 5.6 && voltage_V > 0) {
    ledBlinking = true;
  } else {
    ledBlinking = false;
    digitalWrite(LED_PIN, LOW);
  }

  if (ledBlinking) {
    digitalWrite(LED_PIN, millis() % 500 < 250 ?
    HIGH : LOW);
  }

  // ========== Display on Serial Monitor ==========
  Serial.println("----------------------------");
  Serial.print("Reading #");
  Serial.println(readingCount);
```

```
  Serial.print("Current: ");
  Serial.print(current_A, 2);
  Serial.println(" A");
  Serial.print("Voltage: ");
  Serial.print(voltage_V, 3);
  Serial.println(" V");
  Serial.print("Power:   ");
  Serial.print(Power_W, 2);
  Serial.println(" W");

  // ========== Log to SD Card ==========
  if (sdCardReady) {
    dataFile = SD.open("/datalog.csv", FILE_APPEND);

    if (dataFile) {
      // Write CSV format: Reading,Timestamp,Current,
      // Voltage,Power
      dataFile.print(readingCount);
      dataFile.print(",");
      dataFile.print(timestamp);
      dataFile.print(",");
      dataFile.print(current_A, 4);
      dataFile.print(",");
      dataFile.print(voltage_V, 4);
      dataFile.print(",");
      dataFile.println(Power_W, 3);

      dataFile.close();
      Serial.println("-> Saved to SD card");
    } else {
      Serial.println("-> ERROR: Could not open file!");
    }
  } else {
    Serial.println("-> SD card not available");
  }

  Serial.println();
  delay(100);  // Read every second
}
```

DEPARTMENT OF INDUSTRIAL AND MATERIALS SCIENCE
CHALMERS UNIVERSITY OF TECHNOLOGY
Gothenburg, Sweden
www.chalmers.se

CHALMERS
UNIVERSITY OF TECHNOLOGY